On the Optimization of Compressibility and Hardenability of Sinter-Hardenable PM Steels

NICOLAS GIGUÈRE and CARL BLAIS

Sinter-hardenable steel powders eliminate the extra steps normally required for heat treating since they allow for direct quenching of components at the end of the sintering cycle with a forced convection cooling unit. The current article presents the results of the effect of the alloying method on the optimization of compressibility and sinter-hardenability of sinter-hardenable PM steels. Water-atomized steel powders were produced. Two successive designs of experiments were used to optimize the chemical composition with prealloyed (nickel, chromium, molybdenum, and manganese) and admixed elements (nickel, chromium, manganese, and copper). Static mechanical properties were also characterized. Results show that among all of the combinations of chemical elements and within the range of concentrations studied, the optimum sinter-hardenable powder had the following prealloyed chemistry: 1.5 wt pct Ni, 1 to 1.25 wt pct Mo, and 0.40 to 0.55 wt pct Cr.

DOI: 10.1007/s11661-013-1826-4
© The Minerals, Metals & Materials Society and ASM International 2013

I. INTRODUCTION

IN North America, the automotive industry is the largest consumer of components produced by the powder metallurgy (PM) process. This process is well suited for the mass production of near-net-shaped components. In fact, the average north-American car contains approximately 43 pounds[1] of components made by PM. One of the main challenges of PM is that auto makers continually demand that ferrous PM components have improved dynamic mechanical properties for critical applications such as timing gears, clutch plates, connecting rods, *etc*. This is even more challenging because these high value parts must be produced under ever-increasing pressure to reduce cost. Strategies must therefore be developed to optimize the microstructure and maximize the final density of PM components. Superior mechanical properties are typically obtained with heat treatment, which calls for additional steps in the production sequence, thus increasing the cost adversely and affecting the geometrical conformance of the final part.

In this regard, sinter-hardenable powders certainly show serious potential for the development of high-performance PM components. The approach consists of cooling the parts rapidly enough during the final stage of the sintering cycle to avoid the austenite transforming into pearlite and/or bainite, resulting in a fully martensitic microstructure. Parts are thus quenched at the end of the sintering cycle without the need for reaustenitizing and quenching in a second heat-treatment sequence. The primary advantages of sinter-hardening are[2] no additional heat-treatment steps, reduced distortion which is typically generated by the severity of the oil quench, and no cleaning step after heat treatment. Sinter-hardenability is dictated by the chemistry of the alloy, part density, and the cooling profile of the sintering furnace. Prealloyed chemical elements used to increase hardenability impede compressibility. On the other hand, admixed elements have a less negative effect on compressibility, although they are not as efficient in increasing hardenability, especially in terms of obtaining a homogeneous microstructure. Hence, to fully optimize hardenability and compressibility, a judicious, balanced choice must be made between prealloyed and admixed chemical elements.

The aim of this study was to investigate and model the influence of admixing and prealloying on the optimization of the compressibility and hardenability of sinter-hardenable steel powders. Some of the results presented in the current article can be found in Giguère.[3] A first design of experiments (DOE) was used to sort through eight different variables and a second DOE was then generated to study more precisely the response from the first DOE. Small batches of water-atomized prealloyed steel powders were produced. The latter formed the base material with which powder mixes were prepared through admixing of various fractions of chemical elements also known to increase hardenability. Compressibility and hardenability were characterized by measuring the pressure required to obtain a green density of 6.8 g/cm^3 and the volume fraction of martensite formed upon sinter-hardening. Mechanical properties (transverse rupture strength and apparent hardness) and microstructures were also characterized.

NICOLAS GIGUÈRE, Research Engineer, is with the Centre de Métallurgie du Québec, 3095 Rue Westinghouse, Trois-Rivières, QC G9A5E1, Canada. Contact e-mail: nicolas.giguere@cegeptr.qc.ca CARL BLAIS, Professor, is with the Department of Mining, Metallurgical and Materials Engineering, Université Laval, Room 1728, Adrien-Pouliot Builing, Quebec City, QC G1V 0A6, Canada.
Manuscript submitted March 26, 2012.
Article published online June 25, 2013

II. EXPERIMENTAL PROCEDURE

A. *Water Atomization*

The powders serving as base materials in the current article were produced at Université Laval's Powder Metallurgy Laboratory (LAMPOUL) using a water-atomizer manufactured by Atomising System Ltd. All of the atomizing variables, such as water pressure (70 bars = 1000 psi = 7 MPa), jet angle (45 deg for the primary and 30 deg for secondary), water flow, melt flow, melt temperature, etc. were maintained constant. Melt temperature was 1948 K (1675 °C), which represents a superheat of about 150 K (123 °C). The nozzle diameter in the tundish was 5 mm, and the tundish was preheated to 1473 K (1200 °C). Each batch of powder atomized weighed approximately 20 kg.

B. *Materials Investigated*

Design of experiments was used to minimize the number of experiments while enabling us to determine the influence of each variable. For the first DOE, four chemical elements were prealloyed, and four elements were admixed at two different concentration levels. Two different mathematical models were constructed by measuring the compaction pressure required to obtain a green density of 6.8 g/cm^3 as well as the volume fraction of martensite obtained after sinter-hardening. Table I presents the different variables and levels involved. The subscript "p" and "a" refer to prealloyed and admixed, respectively.

Employing eight variables with two different concentration levels means that 256 experiments (2^8) were required to completely resolve the system. However, a fraction of the design was executed to determine the effect of the eight variables without having to perform 256 experiments. It was possible to reduce the number of experiments to be carried out by performing a 16th of the design, called a 2_{IV}^{8-4}. With this fraction, the eight principal effects could then be characterized; however, these effects were convoluted with statistically negligible triple interactions. This experimental design can be found in Box *et al.*[4] By executing a 16th of this design, the number of experiments was reduced to 16 different mixes/alloys, which are detailed in Table II. A second DOE was generated according to the results obtained in the first phase and will be presented and discussed in Section VI–A.

Table I. Variables Used in the First Design of Experiments and Their Concentration Level

	Concentration Level (wt pct)	
Parameters	Low	High
Ni_p	0	2
Cu_a	1	3
Cr_p	0	2
Mn_a	0	0.5
Mo_p	0	1
Cr_a	0	1
Ni_a	1	3
Mn_p	0	0.5

C. *Powder Processing and Mix Preparation*

Billets of commercially pure iron (0.005 wt pct C, 0.005 wt pct Si, 0.005 wt pct P, and 0.04 wt pct Mn) were used as base material and prealloyed nickel and manganese were added directly in the melt. Chromium and molybdenum were added as ferroalloys. The chemistry of the as-atomized powder was analyzed using atomic absorption. Carbon content before and after sintering was measured using a LECO carbon analyzer (CS600), and oxygen content was measured using another LECO analyzer (TCH600).

Following atomization, hydrogen annealing was performed to lower the powder's oxygen content. Hydrogen annealing was done in an atmosphere of 80 vol pct H_2-20 vol pct N_2 for 60 minutes at 1373 K (1080 °C) for the chromium-containing powders and at 1273 K (1000 °C) for the powders without chromium. The latter heat treatment caused some agglomeration; therefore, a disk pulverizer was used. As this process usually causes strain hardening, the powders were reannealed at 993 K (720 °C) for 1 hour in a nitrogen atmosphere. In order to eliminate size distribution fluctuations from one batch to another, size distribution reconstruction was performed on each powder. Table III presents the chosen size distribution applied to all prealloyed powders. The powder blends were prepared in a V-shape mixer. Admixed elements (Table IV) were added to each mix in proportions determined by DOE. The concentrations of combined carbon and lubricant were maintained constant at 0.7 and 0.75 wt pct, respectively. High chromium alloys tend to experience higher carbon loss. Hence, tests were performed on each base powder to determine the adequate quantity of graphite to be

Table II. Chemical Composition of Mixes/Alloys Dictated by DOE 1

	Chemical Composition (wt pct)							
	Prealloyed Elements				Admixed Elements			
Experiments	Ni	Cr	Mo	Mn	Cu	Mn	Cr	Ni
1	2	2	1	0.5	3	0.5	1	3
2	2	2	0	0	3	0	0	3
3	2	0	0	0.5	3	0.5	0	1
4	2	0	1	0	3	0	1	1
5	2	2	0	0	1	0.5	1	1
6	2	2	1	0.5	1	0	0	1
7	2	0	1	0	1	0.5	0	3
8	2	0	0	0.5	1	0	1	3
9	0	2	1	0	3	0.5	0	1
10	0	2	0	0.5	3	0	1	1
11	0	0	0	0	3	0.5	1	3
12	0	0	1	0.5	3	0	0	3
13	0	2	0	0.5	1	0.5	0	3
14	0	2	1	0	1	0	1	3
15	0	0	1	0.5	1	0.5	1	1
16	0	0	0	0	1	0	0	1

Table III. Particle Size Distribution Used to Reconstruct Atomized Powder Size Distribution

Class (μm)	Fraction (wt pct)
+212	trace
+150	13
+106	22
+75	25
+45	25
−45	15

Table IV. Admixed Constituents

Elements	Brand Name
Nickel	Inco 123
Cr	Acupowder Cr 301
Mn	Acupowder Mn 301
Cu	Acupowder Cu 165
Graphite	PM 1651
Lubricant	Lonza Acrawax "C"

added to obtain 0.7 wt pct in each sinter-hardened test specimen.

D. *Characterization of Density and Flow Rate*

Flow rate and apparent density were measured for each powder blend using a Hall flowmeter apparatus (according to MPIF standards 3 and 4, respectively[5,6]). Compressibility was characterized according to MPIF standard 45 as the pressure required to reach a green density of 6.8 g/cm^3.[7] Finally, green strength was measured by a three-point bend test according to MPIF standard 15.[8]

E. *Pressing and Sintering*

TRS bars (3.17 × 1.27 × 0.635 mm) were pressed to a green density of 6.8 g/cm^3 according to MPIF standards 10 and 41[9,10] and sintered in an Abbott 4-in. continuous belt furnace at 1403 K (1130 °C) for 30 minutes using a 90 vol pct N_2 - 10 vol pct H_2 atmosphere. Fan speed in the forced convection cooling unit (Varicool) was set at 40 Hz which resulted in a cooling rate of 2.0 K/s between 923 K (650 °C) and 573 K (300 °C). Following sinter-hardening, the samples were tempered at 473 K (200 °C) for 1 hour in a nitrogen atmosphere. Finally, sintered density and dimensional change were characterized according to MPIF standards 42 and 44.[11,12]

F. *Characterization of Static Mechanical Properties*

Transverse rupture strength (three point bend test) was characterized according to MPIF standards 43[13] and apparent hardness was measured.

G. *Microstructural Characterization*

Optical microscopy was used to characterize the microstructure of the sintered specimens and to evaluate the volume fraction of martensite. Scanning electron microscopy (SEM) was used to observe the morphology of the atomized powders and phases present. Finally, an electron probe (EPMA) was used to determine the chemical composition of the different phases found in the various microstructures and to obtain elemental X-ray maps.

III. RESULTS OF THE FIRST DOE

A. *Chemical Composition Analysis of Sintered Compacts*

After sintering, chemical compositions of the compacts were analyzed using atomic absorption. Results are presented in Table V. As can be seen, most of the chemical compositions were respected. However, manganese lost was experienced.

B. *Compressibility*

A compressibility curve was generated for each of the aforementioned mixes. The pressure required to obtaining a green density of 6.8 g/cm^3 was used to quantify the effect of admixing and prealloying on compressibility. Table VI presents the results.

As seen in this table, the admixed elements had a negligible effect on the compaction pressure required to obtain a green density of 6.8 g/cm^3, which in turn reflected on the mathematical model linking compressibility to the alloying method. The equation was obtained by performing a least squares regression to fit a model on statistical data. ANOVA testing and confidence intervals were calculated to insure a statistically relevant model. After eliminating the statistically insignificant parameters, a scaled model and an unscaled model were obtained. The scaled equation (obtained with reduced and centered values) was used to determine the relative weight of each parameter, while the unscaled model was used to make predictions (Section IV–D). The final scaled and unscaled equations (R^2 = 0.93) determining the effect of alloying elements on compressibility are presented in Eqs. [1] and [2]:

$$P_{@6.8\ \mathrm{g/cm^3}} = 521.9 + 22.5\mathrm{Ni_p} + 77.3\mathrm{Cr_p} + 15.2\mathrm{Mo_p}\ \text{(scaled)} \quad [1]$$

$$P_{@6.8\ \mathrm{g/cm^3}} = 410.5 + 21.8\mathrm{Ni_p} + 74.9\mathrm{Cr_p} + 29.5\mathrm{Mo_p}\ \text{(unscaled)} \quad [2]$$

The model indicates that only the prealloyed elements had a significant effect on compressibility. It is important to note that these models apply only for the composition intervals presented in Table I. Thus, the scaled model predicted that chromium had the greatest effect on reducing compressibility, followed by nickel and molybdenum.

Table VII presents the flow rate and apparent density of the various prealloyed powders without admixed elements.

Table V. Chemical Compositions of Sintered Compacts Measured by Atomic Absorption Including Both Prealloyed and Admixed Elements

	Chemical Composition (wt pct)					
	Ni	Cr	Mo	Mn	Cu	C
A1	5.02	3.06	0.92	0.82	3.02	0.68
A2	3.03	2.06	0.92	0.45	0.98	0.67
B1	5.01	2.12	—	—	2.97	0.71
B2	3.01	3.11	—	0.44	1.01	0.68
C1	3.00	—	—	0.81	2.97	0.70
C2	4.98	0.96	—	0.37	1.04	0.69
D1	2.99	0.99	1.04	—	3.00	0.69
D2	4.97	—	1.04	0.43	1.03	0.72
E1	1.00	2.08	1.08	0.46	3.03	0.67
E2	2.97	2.82	0.99	—	1.00	0.68
F1	0.98	2.99	—	0.41	3.01	0.66
F2	2.98	1.99	—	0.91	0.98	0.66
G1	3.00	—	1.08	0.41	2.95	0.69
G2	1.04	0.95	1.08	0.89	1.01	0.67
H1	3.06	1.02	—	0.48	3.01	0.71
H2	1.04	—	—	—	1.00	0.70

Table VI. Powder Blend and Compressibility

	Elements (wt pct)		Pressure at 6.8 g/cm^3 (MPa)
	Prealloyed	Admixed	
A1	2Ni-2Cr-1Mo-0.5Mn	3Cu-0.5Mn-1Cr-3Ni	635
A2	2Ni-2Cr-1Mo-0.5Mn	1Cu-1Ni	635
B1	2Ni-2Cr	3Cu-3Ni	579
B2	2Ni-2Cr	1Cu-0.5Mn-1Cr-1Ni	607
C1	2Ni-0.5Mn	3Cu-0.5Mn-1Ni	497
C2	2Ni-0.5Mn	1Cu-1Cr-3Ni	486
D1	2Ni-1Mo	3Cu-1Cr-1Ni	458
D2	2Ni-1Mo	1Cu-0.5Mn-3Ni	452
E1	2Cr-1Mo	3Cu-0.5Mn-1Ni	607
E2	2Cr-1Mo	1Cu-1Cr-3Ni	607
F1	2Cr-0.5Mn	3Cu-1Cr-1Ni	552
F2	2Cr-0.5Mn	1Cu-0.5Mn-3Ni	552
G1	1Mo-0.5Mn	3Cu-3Ni	430
G2	1Mo-0.5Mn	1Cu-0.5Mn-1Cr-1Ni	469
H1	pure Fe	3Cu-0.5Mn-1Cr-3Ni	403
H2	pure Fe	1Cu-1Ni	381

From this table, it was determined that the powders prealloyed with chromium (*i.e.,* A, B, E, and F) tended to have a lower apparent density and a slower flow rate.

Figure 1 presents the results of green strength characterization for the 16 powder mixes identified in Table II. Each specimen was pressed to a green density of 6.8 g/cm^3.

Again, the chromium-prealloyed mixes (A, B, E, and F) presented different properties compared with the chromium-free mixes. The difference in green strength, flow rate, and apparent density can be partially explained by the morphology of the prealloyed powders. Figure 2 presents micrographs highlighting the overall appearance of a prealloyed powder with and without chromium.

Table VII. Apparent Density and Flow Rate of the Water-Atomized Prealloyed Powders

	Prealloyed Elements (wt pct)	Apparent Density (g/cm^3)	Flow Rate (seconds)
A	2Ni-2Cr-1Mo-0.5Mn	2.20	40
B	2Ni-2Cr	2.56	33
C	2Ni-0.5Mn	3.16	24
D	2Ni-1Mo	2.93	26
E	2Cr-1Mo	2.64	30
F	2Cr-0.5Mn	2.74	29
G	1Mo-0.5Mn	3.20	23
H	pure Fe	2.88	26

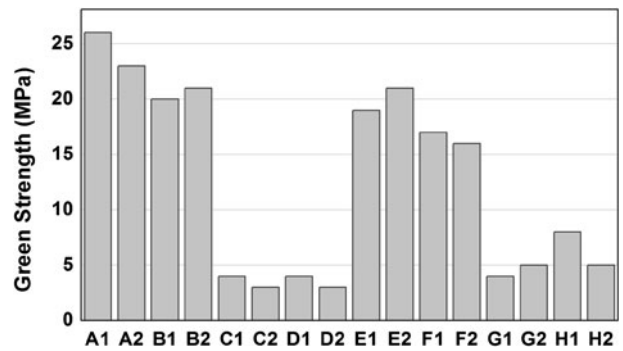

Fig. 1—Green strength of the 16 mixes identified in Table II (0.7 wt pct C, 0.75 wt pct lubricant, green density = 6.8 g/cm^3).

As can be seen in the micrographs in Figure 2, for identical particle size distribution, the powder prealloyed with chromium (Figure 2(a)) showed a significant amount of particles made from the agglomeration of multiple smaller particles and ligaments. Therefore, the particles in the powders prealloyed with chromium were generally more irregular than were those in the chromium-free prealloyed powders. This characteristic explains the significant differences observed for the Cr-bearing powders in terms of apparent density, flow rate, and green strength. Indeed, it is well known that because of interlocking in loose powders or green compacts, irregular particles display lower apparent density, and flow rate and higher green strength.

Another significant aspect related to the presence of chromium in low-alloyed steel powders is its high reactivity toward oxygen. Moreover, unlike less stable oxides such as Fe_xO_y, NiO, or MoO_3, Cr_2O_3 once formed is difficult to reduce during atmosphere sintering.[14] It is therefore not uncommon to see Cr-bearing powders with a residual oxygen concentration significantly higher than that of other PM steels unalloyed with chromium. Table VIII presents the results of the residual oxygen concentration in the hydrogen-annealed prealloyed powders. It can be seen that the presence of chromium in the steel powder strongly affected the residual oxygen content.

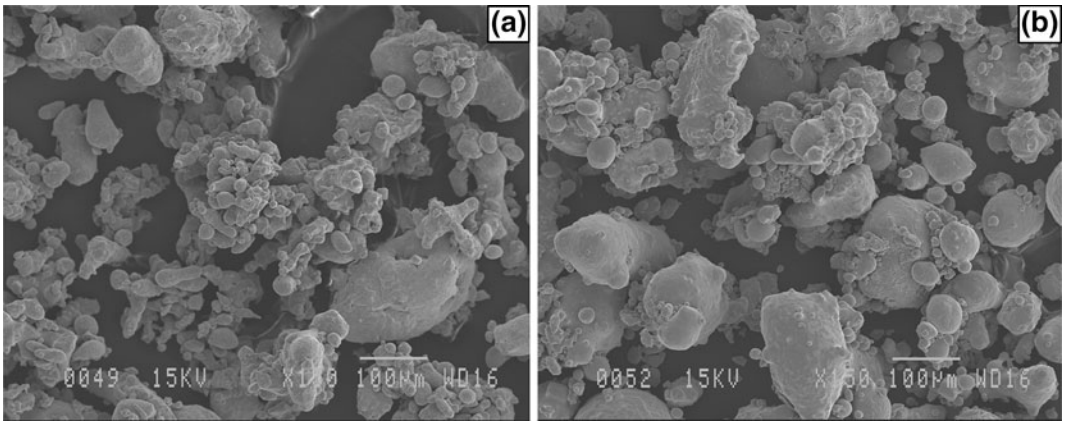

Fig. 2—Overall appearance of prealloyed powder with (*a*) prealloyed chromium (powder F) and (*b*) without chromium (powder H).

Table VIII. Residual Oxygen Concentration in Hydrogen-Annealed Prealloyed Powders

Powders	Elements (wt pct)	O_2 (wt pct)
A	2Ni-2Cr-1Mo-0.5Mn	0.37
B	2Ni-2Cr	0.38
C	2Ni-0.5Mn	0.19
D	2Ni-1Mo	0.09
E	2Cr-1Mo	0.49
F	2Cr-0.5Mn	0.45
G	1Mo-0.5Mn	0.16
H	pure Fe	0.07

C. *Sinter-Hardenability*

Upon sinter-hardening, image analysis was used to analyze the volume fraction of martensite. The microstructure appeared uniform throughout the bars. Figure 3 shows typical microstructures.

The first example is from sample A2 (Figure 3(a)) which shows martensite, nickel-rich areas, and porosity. Characterization of the volume fraction of martensite using image analysis under optical microscopy revealed that the latter composed 98 pct of the microstructure (excluding porosity). In the second example, sample F2 (Figure 3(b)) shows martensite, bainite, pearlite, nickel-rich areas, and porosity. The martensite fraction comprised 69 pct of the pore-free microstructure. Table IX presents the results of image analysis for all 16 series obtained by characterizing at least 20 fields per sample at a magnification of 200 times magnification.

A stepwise backward least squares regression analysis ($\alpha = 0.1$) was performed using the data in Table IX. ANOVA testing and confidence intervals were calculated to insure a statistically relevant model. Following the elimination of statistically insignificant parameters, the final scaled and unscaled models ($R^2 = 0.56$) predicting the influence of alloying elements on hardenability are presented by Eqs. [3] and [4]:

$$\text{Martensite pct} = 76.0 + 12.6\text{Ni}_\text{p} + 11.2\text{Cr}_\text{p} + 10.8\text{Mo}_\text{p}\ \text{(scaled)} \quad [3]$$

$$\text{Martensite pct} = 42.5 + 12.2\text{Ni}_\text{p} + 10.8\text{Cr}_\text{p} + 20.8\text{Mo}_\text{p}\ \text{(unscaled)} \quad [4]$$

According to this scaled model, all of the significant parameters were prealloyed elements (Ni, Cr, and Mo). Arguably, these numbers indicate that prealloyed Ni, Cr, and Mo produced similar effects on hardenability. No admixed elements appeared to have any significant effect on the sinter-hardenability when prealloyed elements were present. At first glance, the R^2 value may seem low. Nevertheless, hardenability of PM steels is a function of not only the concentrations in alloying elements but also of sintered density. Although green density of the test specimens was kept constant, sintered density varied. Thus, thermal conductivity varied accordingly. This situation explains for the most part the apparent divergence of the model.

D. *Mechanical Properties*

In addition to compressibility and hardenability, mechanical properties (transverse rupture strength and apparent hardness) were characterized (Figures 4 and 5).

As can be seen in Figure 4, alloy A2 showed the highest transverse rupture strength. The remaining series was divided into two groups of powder blends having similar mechanical properties. The first group made of blends prepared with powders B, D, E, and F shows intermediate mechanical properties, while the second made from mixes C, G, and H shows the lowest strength values. These properties correlated significantly well with apparent hardness shown in Figure 5.

IV. DISCUSSION FOR THE FIRST DOE

A. *Compressibility*

The scaled model obtained for compressibility shows that prealloyed nickel, chromium, and molybdenum were the only elements to have a statistically significant effect. The strongest effect was from chromium,

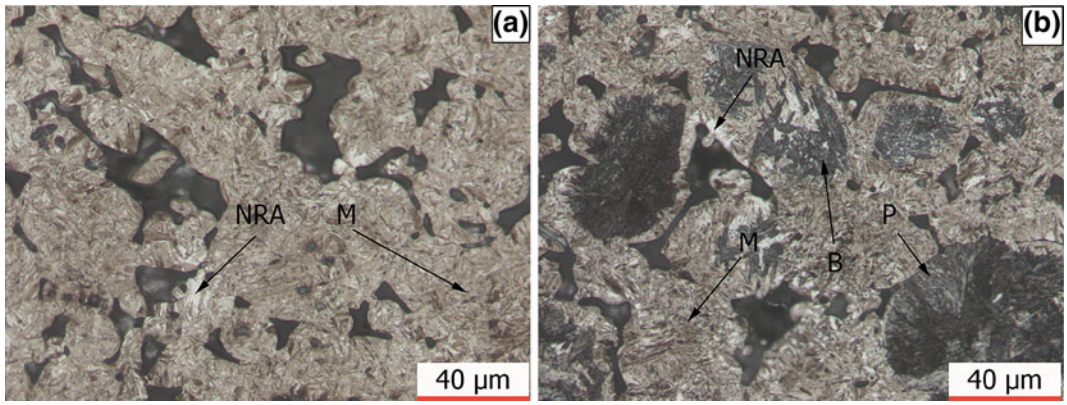

Fig. 3—(*a*) Micrograph of alloy A2 showing a martensitic (M) microstructure with nickel-rich areas (NRA) and (*b*) micrograph of alloy F2 showing a martensitic (M) microstructure with bainite (B), pearlite (P), and nickel-rich areas (NRA). Both specimens were etched with 2 pct Nital, 500 times magnification.

Table IX. Volume Fraction of Martensite as Measured by Image Analysis

Alloys	Volume Fraction of Martensite (pct)
A1	82
A2	98
B1	95
B2	94
C1	73
C2	87
D1	90
D2	87
E1	98
E2	84
F1	75
F2	69
G1	95
G2	57
H1	32
H2	0

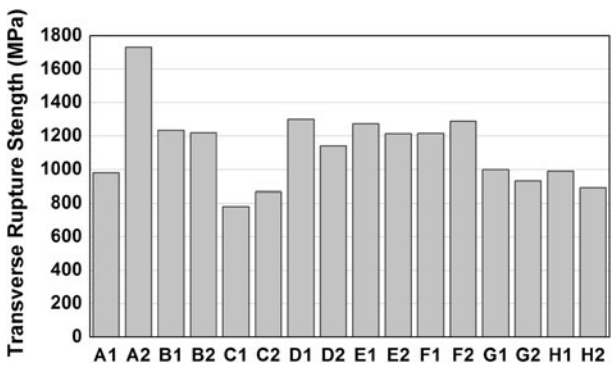

Fig. 4—Transverse rupture strength of samples produced with the powder mixes.

followed by nickel and molybdenum. However, figures widely reported in the literature[15] show a decreased compressibility experienced by an iron powder alloyed

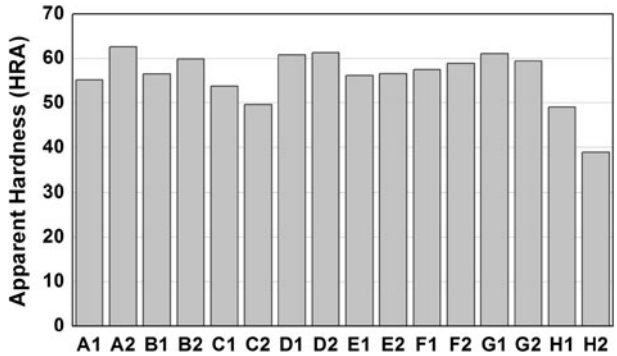

Fig. 5—Apparent hardness samples produced with the powder mixes.

with common transition elements and carbon. Those figures indicate that among the metal groups, manganese should have had the greatest effect on reducing compressibility, followed by nickel, molybdenum, and chromium; however, this is not corroborated by the results presented above. Here, when manganese was prealloyed, 0.5 wt pct was the highest concentration used. At this concentration, manganese should have had the same effect as 2 wt pct prealloyed nickel. This concentration may therefore not have sufficed to significantly affect compressibility. Commercially available powders have similar manganese concentrations and are presented by their manufacturer as having good compressibility. This situation leads us to believe that there exists a minimum concentration threshold under which manganese has a negligible effect on lowering compressibility. Consequently, the linear behavior reported in the literature may not hold true for lower concentrations.

As mentioned earlier, chromium appears to have had the most significant effect on compressibility according to the model obtained. This strong effect by chromium may be explained by its marked affinity with oxygen, resulting in the formation of oxide particles during atomization and/or sintering. As presented in Table VIII, the oxygen content increased drastically with the addition of 2 wt pct

of chromium. High oxygen content results in an increased volume fraction of oxide particles which are known to negatively affect compressibility. Furthermore, differences in particle morphology were observed in the mixes prealloyed with chromium. Indeed, Cr-bearing melts were less fluid upon atomization, which produced a larger fraction of elongated particles (ligaments) rather than spherical particles (Figure 2(a)). Elongated particles had a significant impact on apparent density (lower), green strength (considerably higher), and flow rate (slower), which are all strongly related to particle morphology. Moreover, a lower apparent density requires a higher compaction pressure to obtain a particular green density. These factors thus explain the important effect of prealloyed chromium on compressibility. Finally, the model found no admixed elements with a significant effect on compressibility, which is in accordance with theory.[16]

B. *Sinter-Hardenability*

Sinter-hardenability was characterized by measuring the volume fraction of martensite. The scaled model obtained showed that prealloyed nickel had the strongest effect on hardenability, followed very closely by prealloyed chromium and molybdenum. However, their scaled values are so close that it becomes difficult to actually differentiate their contribution on hardenability.

In carbon steels, the effect of different elements on hardenability can be characterized by the Grossman hardening factor which measures the enhancement effect on the critical quench diameter.[16] Nickel had the lowest effect on hardenability (Grossman hardening factor of 1.4/pct), with chromium and molybdenum displaying a factor of 3.1 and 3.7/pct, respectively; however, this does not take into account the combined effects, whereas this model does. It is well known in wrought steel metallurgy that synergetic effects are observed for certain combinations of alloying elements.[17] It is most likely that such effects took place during this experimentation, thereby modifying the overall effect on the sinter-hardening, compared with powders to which the alloying elements were added independently.[15]

The addition of prealloyed chromium and manganese caused the formation of complex chromium and manganese oxides in the sintered parts, as shown in Figure 6 (see also EDS spectrum in Figure 7) which resulted in less free Cr and Mn to benefit hardenability. Furthermore, a typical chrome-free powder has a typical oxygen content of 0.1 wt pct, while that of a powder prealloyed with Cr is close to 0.4 wt pct. Considering a powder prealloyed with 2 wt pct Cr, and assuming that all of the excess oxygen (*i.e.*, 0.3 wt pct) reacted with the chromium to form Cr_2O_3, only 1.3 wt pct of chromium remained in the solid solution. Thus, only the nonoxidized fraction of the initial chromium participated in increasing hardenability. As for the admixed chromium, it had no significant effect on hardenability primarily because the chromium particles did not sinter and were found almost intact, which confirms that limited diffusion took place in the iron matrix (arrowed areas in Figure 8 as well as in Section IV–C below).

Admixed nickel (1 or 3 wt pct additions) was not found to be a significant factor in improving hardenability. This is because admixed nickel rarely diffuses

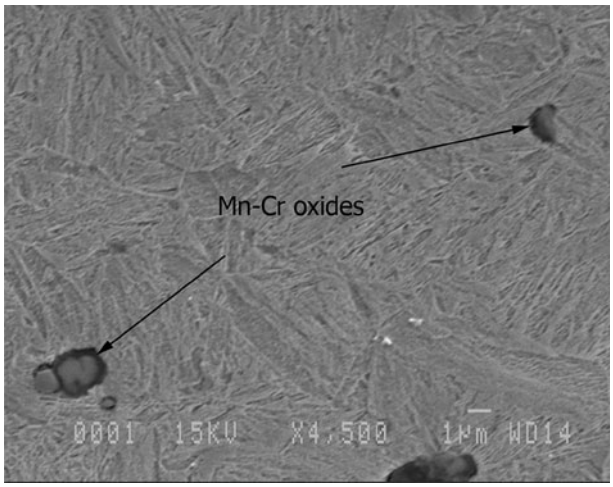

Fig. 6—SEM micrograph showing Mn-Cr oxides.

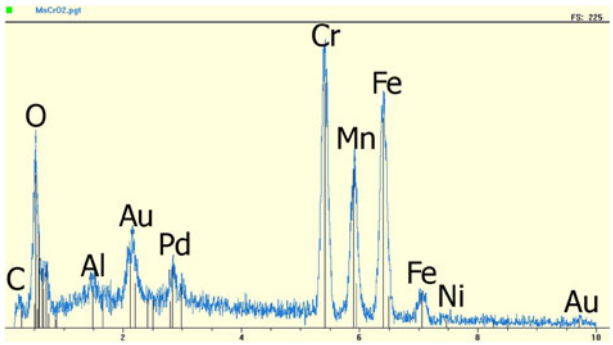

Fig. 7—EDS spectrum of Cr-Mn oxide found (Fig. 6).

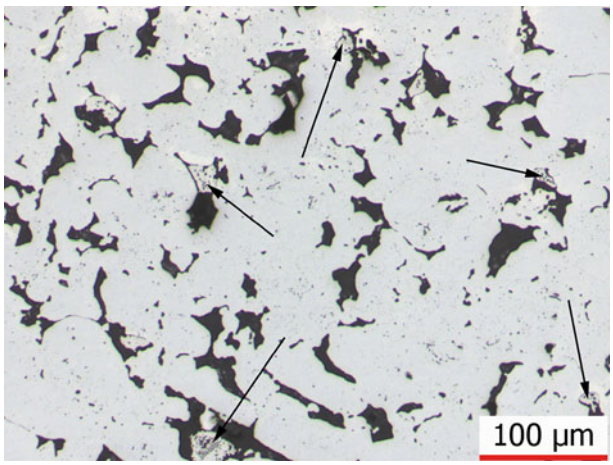

Fig. 8—Optical micrograph showing nonsintered admixed chromium particles, 200 times magnification.

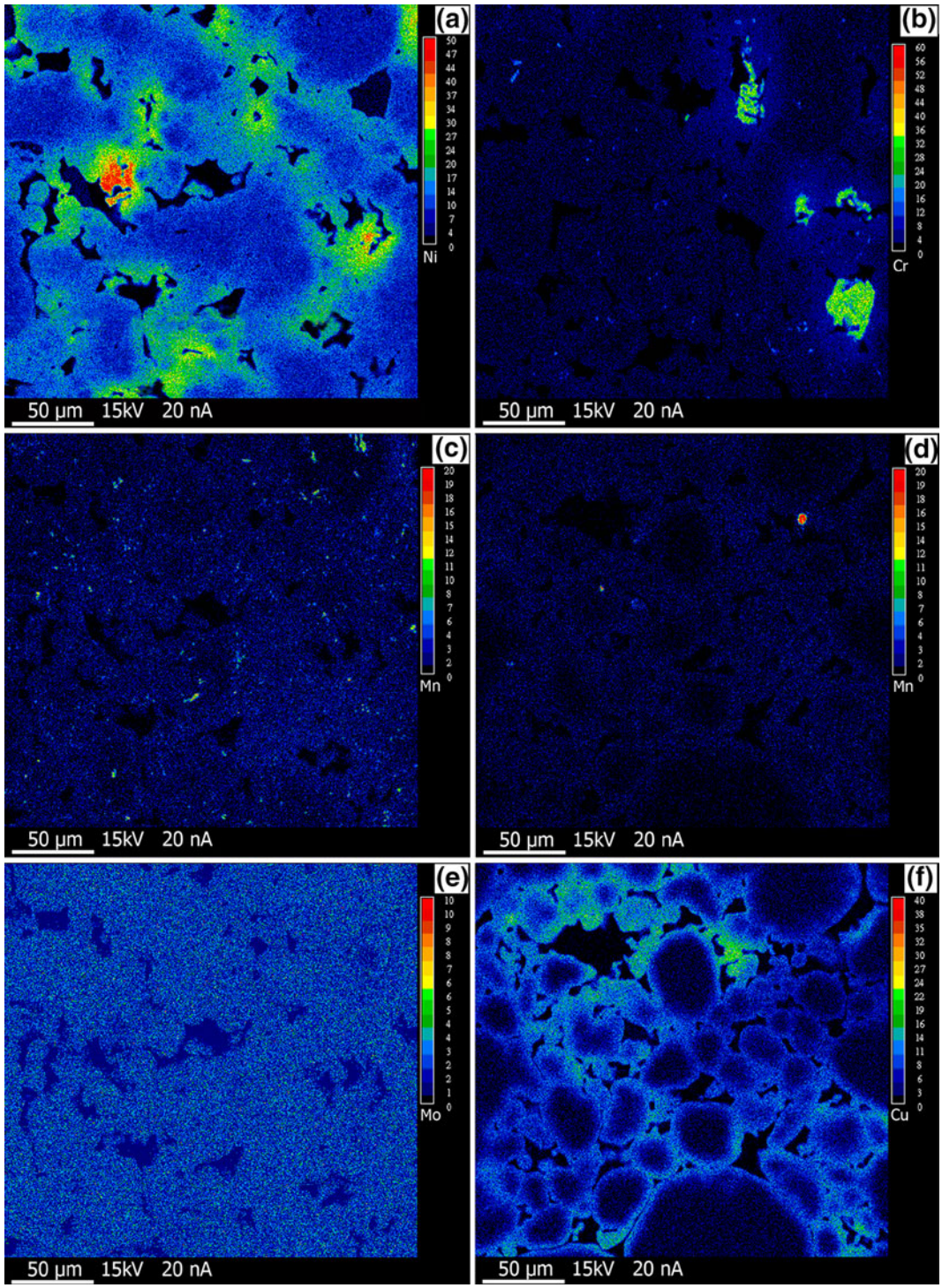

Fig. 9—Elemental mapping obtained from an electron microprobe for (*a*) prealloyed and admixed nickel in alloy A1, (*b*) prealloyed and admixed chromium in alloy F1, (*c*) prealloyed manganese in alloy F1, (*d*) admixed manganese in alloy H1, (*e*) prealloyed molybdenum in alloy A1, and (*f*) admixed copper in alloy A1. 200 times magnification.

homogeneously under typical sinter-hardening conditions leading to the formation of nickel-rich areas. When localized in these areas, nickel cannot contribute significantly to hardenability. It was found that 3 wt pct of admixed Ni produced as much as 15 pct of nickel-rich areas (NRA) and 1 wt pct of admixed nickel produced 2 to 5 pct of NRA. No nickel-rich areas were found in prealloyed powder since nickel is well distributed in prealloyed powders. Prealloyed and admixed manganese up to 0.37 wt pct were also found to have little effect on improving hardenability. This result is attributed to their low concentrations, compared with the other alloying elements, combined with the propensity of manganese to react with oxygen to form oxide inclusions.

C. *EPMA Elemental Mapping*

Using an electron probe microscope, elemental mapping was performed to determine the localization of the prealloyed and admixed elements. Figure 9 presents the results. Only a few images sufficed to explain the distribution of these addition elements.

Figure 9(a) presents the X-ray maps for the prealloyed and admixed nickel. Prealloyed nickel is uniformly distributed within the matrix, as shown by the dark blue coloration. Admixed nickel formed nickel-rich areas and are characterized by the green and yellow portions of the map. These areas are surrounded by light blue areas which indicate that there is a concentration gradient between the admixed Ni particles and the center of the prealloyed particles, meaning that at least some of the admixed nickel diffused into the matrix. This is in accordance with the study of Tougas *et al.*[18]

Figure 9(b) presents the elemental mapping of chromium. It was discussed earlier that admixed chromium did not diffuse (yellow-green on the figure); however, as can be seen in this figure, the admixed chromium did in fact diffuse (bright blue areas around the admixed particles). Prealloyed chromium is dispersed in the iron matrix (dark blue), although some isolated bright blue spots can be seen. These spots, found to be complex Cr-Mn oxides, can be correlated with the prealloyed manganese (Figure 9(c)), where the exact same areas are seen to be rich in manganese. Manganese that did not form oxide inclusions is shown to be uniformly dispersed (dark blue in Figure 9(c)). Interestingly, the admixed manganese (Figure 9(d)) diffused well into the iron matrix, producing very few manganese oxide particles. The prealloyed molybdenum was found to be uniformly dispersed, as shown in Figure 9(e). Finally, as expected, 3 wt pct of admixed copper (Figure 9(f)) did not diffuse throughout the iron matrix, thereby forming copper rich areas.

D. *Optimization of Compressibility and Sinter-Hardenability*

From compressibility and hardenability models, predictions can be made to find the optimum sinter-hardenable material. There were three unknown variables (Ni_p, Cr_p, and Mo_p) and only two equations. To solve this system, one of the variables had to be kept constant. Moreover, compressibility and hardenability had to be fixed to solve these equations.

According to Lindsley,[19] Ancorsteel 737SH possesses a good combination of compressibility and hardenability. On the 737SH data sheet,[20] a green density of 6.8 g/cm^3 is obtainable with a compaction pressure of 500 MPa (36 tsi). The latter criterion was therefore used to determine the most compressible sinter-hardenable powders among those studied. Similarly, according to Haberberger *et al.*,[21] sinter-hardening materials are characterized by their significant hardenability which enables the transformation of austenite into more than 80 vol pct martensite using accelerated cooling. In this study, the criterion used to discriminate in terms of hardenability was that a powder should show a minimum of 85 vol pct of martensite upon sinter-hardening. To solve this system, nickel content (0, 0,5, 1, 1.5, and 2 wt pct), compaction pressure (500 and 550 MPa) and martensite volume fraction (85, 90, 95, and 100 vol pct) were implemented in the equation system, and prealloyed chromium and molybdenum were determined. The model did produce some results that were outside of the chemical compositions initially used in our design of experiment (0 wt pct $\leq Cr_p \leq$ 2 wt pct, 0 wt pct $\leq Mo_p \leq$ 1 wt pct), thus making them unusable. They are, however, excellent indications as to what other chemistries should be studied in the next phase of our research. Table X presents the alloys respecting the above mentioned conditions.

Table X. Chemical Composition (wt pct) of the Modelized Alloys

	Ni	Cr	Mo	Compaction Pressure at 6.8 g/cm^3 (MPa)	Volume Fraction of Martensite (pct)
1	2	0.95	0.85	550	95
2	2	0.20	1.00	500	90
3	2	1.05	0.55	550	90
4	1.5	1.10	0.85	550	90
5	2	0.35	0.70	500	85
6	1.5	0.40	1.00	500	85
7	2	1.18	0.25	550	85
8	1.5	1.20	0.55	550	85
9	1	1.25	0.80	550	85

As can be seen in Table X, the alloys with more than 1 wt pct of chromium required a higher compaction pressure to reach a green density of 6.8 g/cm^3 (550 MPa) compared with the alloys with less than 0.4 wt pct. The best compromise thus appears to be alloys 2, 5, and 6 which had only a small quantity of prealloyed chromium, 1.5 to 2 wt pct nickel, and between 0.70 and 1 wt pct Mo. These alloys required only 500 MPa to reach a green density of 6.8 g/cm^3 and to yield as much as 85 pct of martensite upon sinter-hardening. Of these three alloys, alloy 6 had the lowest concentration of prealloyed elements and thus constitutes the ideal choice in terms of hardenability and compressibility. This powder does not match any MPIF standards for structural parts, although its chemistry is significantly similar to that of Rio Tinto Metal Powders grade 4701.

V. CONCLUSIONS ON FIRST DOE

In the first part of the current article aimed at modeling the influence of admixing and/or prealloying chemical elements known to increase hardenability on the optimization of compressibility and hardenability of sinter-hardenable steel powders, the main conclusions can be summarized as follows:

1. Within the concentration range studied, the admixed elements known to improve hardenability (*i.e.,* Ni, Cr, and Mo) had no influence on compressibility.

2. Prealloyed chromium displayed the most significant influence in reducing compressibility, followed by nickel and molybdenum. However, it was found that chromium had an indirect effect on particle morphology upon atomizing, which resulted in lower apparent density and compressibility. The influence of chromium must therefore be further examined to eliminate any possible bias brought about by the significant difference in particle morphology between Cr-bearing powders and those without chromium.
3. Contrary to what is reported in the literature,[15] manganese concentrations ranging from 0.3 to 0.4 wt pct have little impact on compressibility or hardenability of sinter-hardenable steel powders.
4. Prealloyed Ni, Cr, and Mo perform similarly in improving the hardenability of sinter-hardenable steel powders.
5. The model generated to optimize the hardenability and compressibility of sinter-hardenable powders indicates that the optimum chemistry is prealloyed: 1.5 wt pct Ni, 0.50 wt pct Cr, and 1.00 wt pct Mo.

VI. RESULTS OF THE SECOND DOE

A. *Second DOE*

Mathematical models obtained with the first DOE demonstrated that, within the chemical composition range studied, nickel, chromium, and molybdenum were the only prealloyed elements with a significant effect on both compressibility and hardenability. Hence, a second design of experiments was conceived around those results.

For the second DOE, prealloyed nickel was maintained constant (1.5 wt pct) as for admixed copper (2 wt pct), graphite (0.7 wt pct after sintering), and lubricant (Lonza Acrawax "C" 0.75 wt pct). Only molybdenum and chromium were tested at two different concentration levels. The DOE proposed is thus a 2^2. A central point was added (powder L), enabling to construct a second degree model if necessary. Powder blends studied with the second DOE are presented in Table XI.

B. *Chemical Composition Analysis of Sintered Compacts*

After sintering, chemical compositions of the compacts were analyzed. Results are presented in Table XII.

Table XI. Chemical Composition of Atomized Powders Serving as Base Material Dictated by the Second DOE

	Chemical Composition (wt pct)		
Powders	Ni	Cr	Mo
J	1.50	0.10	0.50
K	1.50	0.10	2.00
L	1.50	0.55	1.25
M	1.50	1.00	0.50
N	1.50	1.00	2.00

As can be seen, most of the chemical compositions were respected. Carbon loss was more important than expected for high Cr alloys.

C. *Compressibility*

For each base powder presented above, the compaction pressure required to reach a green density of 6.8 g/cm^3 was used to quantify the effect of prealloyed chromium and molybdenum on compressibility. Results are presented in Table XIII.

A mathematical model was obtained by performing a least squares regression to fit a model on statistical data. ANOVA testing and confidence intervals were calculated to insure a statistically relevant model. After eliminating statistically insignificant parameters, a scaled and an unscaled model were obtained. The scaled model (obtained with reduced and centered values) is used to determine the relative weight of each parameters, and the unscaled model is used to make predictions. The final scaled and unscaled models determining the effect of alloying elements on compressibility are given by Eqs. [5] and [6]:

$$P_{@6,8\ \mathrm{g/cm^3}} = 556 + 16.4\mathrm{Mo} + 30.6\mathrm{Cr} + 14.1\mathrm{MoCr}\ \text{(scaled)} \quad [5]$$

$$P_{@6,8\ \mathrm{g/cm^3}} = 520 - 0.15\mathrm{Mo} + 15.7\mathrm{Cr} + 41.5\mathrm{MoCr} \quad [6]$$

It is important to note that these models are applicable uniquely for the composition intervals shown in Table X. The scaled model predicts that chromium has the greatest effect on reducing compressibility, followed by molybdenum, and the interaction between chromium and molybdenum.

Table XII. Chemical Compositions of Sintered Compacts

	Chemical Composition (wt pct)			
	Ni	Cr	Mo	C
J	1.47	0.13	0.6	0.68
K	1.43	0.11	2	0.71
L	1.45	0.54	1.3	0.68
M	1.42	1.1	0.59	0.66
N	1.43	1.12	2.02	0.67

Table XIII. Compaction Pressure Required to Reach a Green Density of 6.8 g/cm^3 for Each Powder Blend Studied (Standard Deviation in Parenthesis)

	Elements (wt pct)		Pressure@ 6.8 g/cm^3
	Prealloyed	Admixed	MPa
J	1.5Ni-0.5Mo-0.1Cr	2Cu	524 (4)
K	1.5Ni-2Mo-0.1Cr	2Cu	530 (4)
L	1.5Ni-1.25Mo-0.55Cr	2Cu	553 (5)
M	1.5Ni-0.5Mo-1Cr	2Cu	557 (5)
N	1.5Ni-2Mo-1Cr	2Cu	619 (5)

Table XIV. Residual Oxygen Concentration in Hydrogen-Annealed Prealloyed Powders

Powders	Elements (wt pct)	O_2 (wt pct)
J	1.5Ni-0.5Mo-0.1Cr	0.21*
K	1.5Ni-2Mo-0.1Cr	0.19*
L	1.5Ni-1.25Mo-0.55Cr	0.25*
M	1.5Ni-0.5Mo-1Cr	0.38**
N	1.5Ni-2Mo-1Cr	0.27**

*1318 K (1045 °C), 60 minutes, 80 pct-vol H_2-20 pct-vol N_2.
**1353 K (1080 °C), 60 minutes, 80 pct-vol H_2-20 pct-vol N_2.

Table XV. Apparent Density and Flow Rate of the Water-Atomized Prealloyed Powders

	Powders (wt pct)	Apparent Density (g/cm^3)	Flow Rate(s)
J	1.5Ni-0.5Mo-0.1Cr	3.20	22
K	1.5Ni-2Mo-0.1Cr	3.15	26
L	1.5Ni-1.25Mo-0.55Cr	3.25	25
M	1.5Ni-0.5Mo-1Cr	3.40	24
N	1.5Ni-2Mo-1Cr	3.58	22

As observed in the first series, powders with the lower chromium concentrations levels were easier to deoxidize when treated under hydrogen (Table XIV).

Physical properties of the atomized powders were also characterized. Table XV presents the flow rate and apparent density of the various prealloyed powders without admixed elements.

Compared with the first series of experiments, where a different morphology had been noticed between two categories of atomized powders, the second DOE produced powders with similar apparent density and flow rate. However, powders containing 1 pct of prealloyed Cr showed again a higher apparent density. Moreover, the chemical compositions intervals studied during for the second DOE are much more restrained, which produces closer results. The same observation will be made concerning mechanical properties and sinter-hardenability.

Green strength for a green density of 6.8 g/cm^3 was evaluated. Results are presented in Figure 10.

The five powders have a similar green strength, excepted for powder M. However, no differences in powder morphology were observed as shown in Figure 11.

D. *Sinter-Hardenability*

Specimens were sintered in 4-in. continuous belt furnace (Abbott) at 1403 K (1130 °C) for 30 minutes using a 90 vol pct N_2 - 10 vol pct H_2 atmosphere. The speed of the fan in the forced convection cooling unit (Varicool) was turned off since specimens were all fully martensitic when the Varicool was on. The latter cooling condition resulted in a cooling rate of 0.7 K/s between 923 K (650 °C) and 573 K (300 °C). Upon sinter-hardening, the volume fraction of martensite was

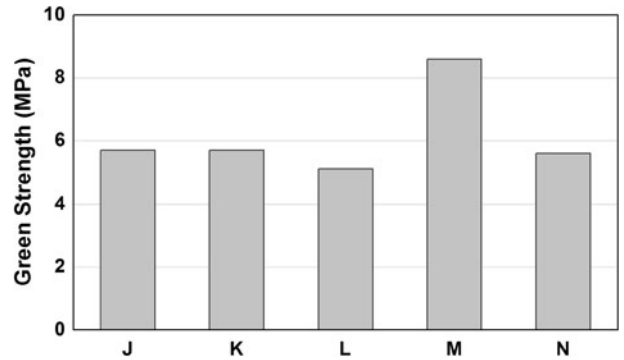

Fig. 10—Green strength for mixes dictated by the second DOE: J = 0.5 wt pct Mo and 0.1 wt pct Cr; K = 2 wt pct Mo and 0.1 wt pct Cr; L = 1.25 wt pct Mo and 0.55 wt pct Cr; M = 0.5 wt pct Mo and 1 wt pct Cr; and N = 2 wt pct Mo and 1 wt pct Cr.

measured using image analysis. A typical microstructure of a specimen made using powder J (1.5 wt pct Ni, 0.10 wt pct Cr, and 0.5 wt pct Mo) is presented in Figure 12.

Results of image analysis are presented in Table XVI (convection cooling unit turned off). Using the data in Table XVI, a mathematical model was obtained. Martensite volume fraction was analyzed on samples cooled without using the forced convection unit.

$$\text{pct Martensite} = 95.1 + 3.4\text{Mo} + 4.8\text{Cr} + 2.7\text{MoCr (scaled)} \quad [7]$$

$$\text{pct Martensite} = 78.5 + 8.7\text{Mo} + 20.7\text{Cr} - 8.0\text{MoCr} \quad [8]$$

Unfortunately, this model is not significant. Its R^2 is good (0.81), but the model does not pass the ANOVA ($F_{\text{model}} = 1.45 \leq F_\alpha = 215$), which means the model reveals itself as being statistically insignificant. All imaginable permutations were tried to fit a model on these data, but the chemical intervals studied are so small that values obtained for each alloy are very close to each other and are difficult to differentiate.

E. *Mechanical Properties*

Along with compressibility and sinter-hardenability, mechanical properties (transverse rupture strength and apparent hardness) were characterized for the slowest cooling rate condition, *i.e.*, when the convection cooling unit was turned off. Figure 13 shows the transverse rupture strength of all five alloys.

From Figure 13, it can be seen that transverse rupture strength does not show a high fluctuation form powders J to N. Powder J has the higher resistance followed by powders K and L. The higher chromium contents of powders M and N produced hard and brittle chromium oxides in the microstructure, lowering the transverse rupture strength.

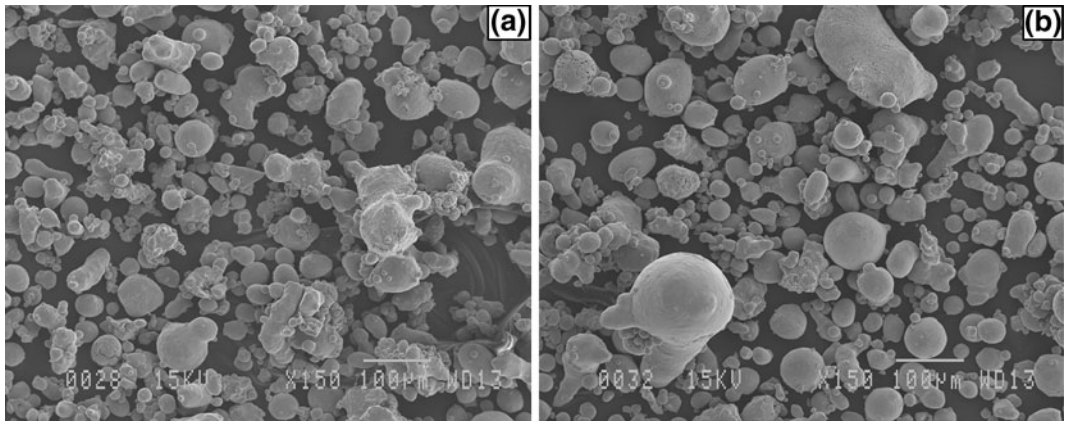

Fig. 11—Morphologies of powders K and M atomized and heat treated.

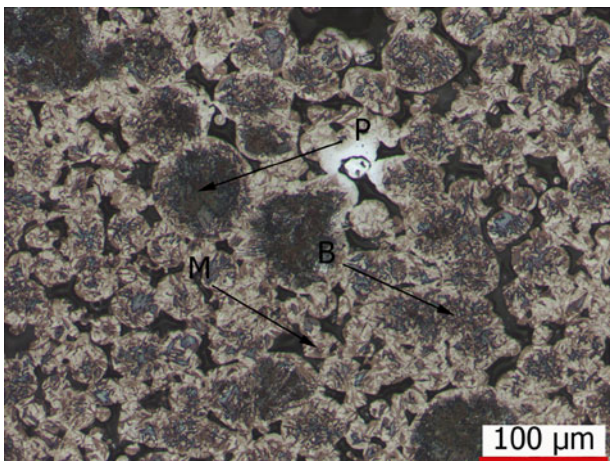

Fig. 12—Micrograph of alloy J showing a martensitic (M) microstructure with bainite (B) and fine perlite (P), etched in 2 pct Nital, 200 times magnification.

Table XVI. Martensite Volume Fraction as Measured Using Image Analysis (Standard Deviation in Parenthesis)

Alloys	Martensite Volume Fractions (pct)
J	82.9 (0.8)
K	93.0 (0.9)
L	99.7 (1.0)
M	98.5 (1.0)
N	99.6 (1.0)

Apparent hardness was also measured for all alloys. Results are presented in Figure 14. Powders J and K with low concentrations of alloying elements have the lower apparent hardness. Powders L, M, and N do not have a significantly different hardness.

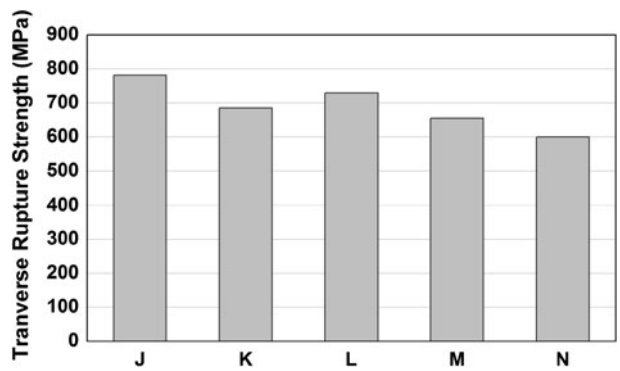

Fig. 13—Transverse rupture strength of the alloys studied.

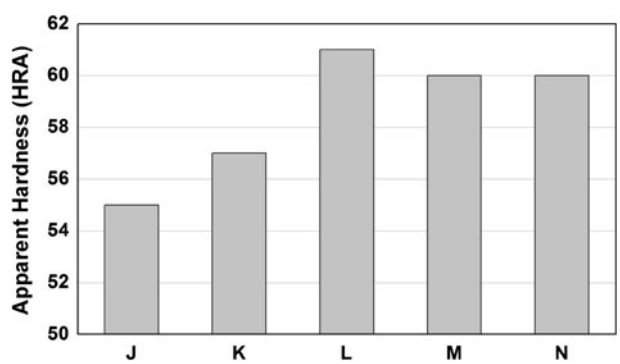

Fig. 14—Apparent hardness for all five powders.

F. *Optimization of Compressibility and Sinter-Hardenability*

With no significant model for sinter-hardenability, it is not possible to develop an equation that would optimize both compressibility and sinter-hardenability. To solve this problem, results for each powder/alloy

Table XVII. Table Showing Compressibility and Sinter-Hardenability Results for Each Powder

Powder/Alloy	Compaction Pressure to 6.8 g/cm^3 (MPa)	Martensite Volume Fraction (pct)
J	524	82.9
K	530	93.0
L	553	99.7
M	557	98.5
N	619	99.6
Mean	556.6	94.7
Standard Deviation	37.7	7.2

Table XVIII. Scaled Values for Compressibility and Sinter-Hardenability

	Compressibility	Sinter-Hardenability	$\sum i$
J	0.87	−1.65	0.78
K	0.71	−0.24	0.47
L	0.10	0.69	0.79
M	−0.01	0.52	0.51
N	−1.66	0.68	−0.98

(J, K, L, M, and N) were compared with the mean and the standard deviation of each criterion, *i.e.*, compressibility and volume fraction of martensite. In fact, results were scaled to find the optimum combination of compressibility and sinter-hardenability. Results for each criterion are presented in Table XVII along with their mean and standard deviation.

The values of Table XVII were scaled following Eq. [9]:

$$z = \frac{x - \overline{x}}{\sigma} \qquad [9]$$

This way, the relative weight of each result was evaluated. For example, if a result is above average but the standard deviation is wide, then its relative weight is less than that for a result above average with a narrow standard deviation. Results for each calculated relative weight for each powder/alloy for each criterion are presented in Table XVIII.

Usually, a scaled value above one indicates that the property measured compares favorably with the mean. However, in the case of compressibility, a minus sign was added in front of the scaled value to reflect the fact that better compressibility is characterized by low compacting pressures. Since the optimization is performed by adding up the scaled values (the highest summation being the best powder/alloy), a lower compaction pressure is a beneficial. Table XVIII should be read knowing that the more a summation is far from 0, the more it stands favorably (+) or negatively (−) apart.

From Table XVIII, one can see regarding compressibility that powder J, which was the most compressible, gets a scaled value of 0.87. On the other hand, powder N, the least compressible among all, gets a scaled value of −1.66. Same rationale may be applied to sinter-hardening values. The highest summation of the two scaled values gives the best compromise between compressibility and sinter-hardenability. Therefore, from these five powders/alloys, the composition that optimized both chemistry and compressibility is that of powder L, which is 1.5 wt pct Ni, 1.25 wt pct Mo, and 0.55 wt pct Cr.

VII. CONCLUSIONS ON SECOND DOE

The DOE used for the second phase was developed to study the effect of prealloyed molybdenum and chromium on the optimization of compressibility and sinter-hardenability, while keeping the nickel content constant. The main conclusions of this research can be summarized as followed:

1. Within the concentration range studied, prealloyed chromium has the most influence on reducing compressibility followed by molybdenum and the second degree interaction between chromium and molybdenum.
2. A nonsignificant model was obtained for sinter-hardenability. This result is attributed to the narrow composition interval studied.
3. Optimization was held using the summation of scaled values. From this, we conclude that the chemical composition optimizing both compressibility and sinter-hardenability is 1.5 wt pct Ni, 1.25 wt pct Mo, and 0.55 wt pct Cr.

VIII. GENERAL CONCLUSIONS

The aim of the current article was to study the effect of the alloying method (prealloying and admixing) on the optimization of compressibility and sinter-hardenability of water-atomized sinter-hardenable steel powders. Mechanical properties were also characterized.

Design of experiments (DOE) was used to minimize the number of experiments while enabling the determination the influence of each significant variable on both compressibility and sinter-hardenability.

The two series of experiments allowed us to determine a chemical composition that optimizes compressibility and sinter-hardenability. This chemistry is as follows: 1.5 wt pct Ni, 1 to 1.25 wt pct Mo, and 0.40 to 0.55 wt pct Cr.

ACKNOWLEDGMENTS

This research was funded by the Auto21-Network of Centers of Excellence, Canada.

REFERENCES

1. M. Lutheran: *Int. J. Powder Metall.*, 2010, vol. 46, pp. 25–28.
2. G.F. Bocchini, B. Rivolta, G. Silva, E. Poggio, M.R. Pinasco, and M.G. Ienco: *Powder Metall.*, 2004, vol. 47, pp. 343–51.

3. N. Giguère and C. Blais: *Mater. Sci. Forum*, 2012, vols. 706–709, pp. 2107–11.
4. G.E.P. Box, W.G. Hunter, and J.S. Hunter: *Statistics for Experimenters*, Wiley, New York, NY, 1978, pp. 307–44.
5. MPIF: *Metal Powder Industries Federation, Standard 3*, Metal Powder Industries Federation, Princeton, NJ, 1998.
6. MPIF: *Metal Powder Industries Federation, Standard 4*, Metal Powder Industries Federation, Princeton, NJ, 1998.
7. MPIF: *Metal Powder Industries Federation, Standard 45*, Metal Powder Industries Federation, Princeton, NJ, 1998.
8. MPIF: *Metal Powder Industries Federation, Standard 15*, Metal Powder Industries Federation, Princeton, NJ, 1998.
9. MPIF: *Metal Powder Industries Federation, Standard 10*, Metal Powder Industries Federation, Princeton, NJ, 1998.
10. MPIF: *Metal Powder Industries Federation, Standard 41*, Metal Powder Industries Federation, Princeton, NJ, 1998.
11. MPIF: *Metal Powder Industries Federation, Standard 42*, Metal Powder Industries Federation, Princeton, NJ, 1998.
12. MPIF: *Metal Powder Industries Federation, Standard 44*, Metal Powder Industries Federation, Princeton, NJ, 1998.
13. MPIF: *Metal Powder Industries Federation, Standard 43*, Metal Powder Industries Federation, Princeton, NJ, 1998.
14. D.R. Gaskell: *Introduction to Metallurgical Thermodynamics*, 2nd ed., Hemisphere Publishing Corp., New York, NY, 1981, p. 247.
15. R.M. German: *Powder Metallurgy & Particulate Materials Processing*, Metal Powder Industries Federation, Princeton, 1994, pp. 194–96.
16. E. Klar: *ASM Handbook Volume 7: Powder Metallurgy*, 6th ed., American Society for Metals, Metals Park, OH, 1997, pp. 311–20.
17. G. Krauss: *Steels: Processing, Structure and Performance*, ASM International, Materials Park, OH, 2005, pp. 297–325.
18. B. Tougas, C. Blais, F. Chagnon, and S. Pelletier: *Metall. Mater. Trans. A*, 2013, vol. 44A, pp. 754–65.
19. B. Lindsley: *Euro PM2007*, Toulouse, France, 2007, pp. 6.
20. *Technical Data*, 2004. http://www.hoeganaes.com/Product%20Datasheets/DatasheetsJan2009/Ancorsteel737SH.pdf.
21. T. Haberberger, F.G. Hanejko, M.L. Marucci, and P. King: *Properties and Applications of High Density Sinter-Hardening Materials*, 2006. http://www.hoeganaes.com/TechPapersv2/124.pdf.